Earth **Surface**
Dynamics

Clast imbrication in coarse-grained mountain streams and stratigraphic archives as indicator of deposition in upper flow regime conditions

Fritz Schlunegger and Philippos Garefalakis

Institute of Geological Sciences, University of Bern, Bern, Switzerland

Correspondence: Fritz Schlunegger (fritz.schlunegger@geo.unibe.ch) and Philippos Garefalakis
(philippos.garefalakis@geo.unibe.ch)

Abstract. Clast imbrication is one of the most conspicuous sedimentary structures in coarse-grained clastic deposits of modern rivers but also in the stratigraphic record. In this paper, we test whether the formation of this fabric can be related to the occurrence of upper flow regime conditions in streams. To this end, we calculated the Froude number at the incipient motion of coarse-grained bedload for various values of relative bed roughness and stream gradient as these are the first-order variables that can practically be extracted from preserved deposits. We found that a steeper energy gradient, or slope, and a larger bed roughness tend to favor the occurrence of supercritical flows. We also found that, at the onset of grain motion, the ratio ϕ between the critical shear stress for the entrainment of a sediment particle and its inertial force critically controls whether flows tend to be super- or subcritical during entrainment. We then mapped the occurrence of clast imbrication in Swiss streams and compared these data with the hydrologic calculations. Results indicate that imbrication may record supercritical flows provided that (i) ϕ values are larger than ca. 0.05, which is appropriate for streams in the Swiss Alps; (ii) average stream gradients exceed ca. $0.5 \pm 0.1°$; and (iii) relative bed roughness values, i.e., the ratio between water depth d and bed sediment D_{84}, are larger than $\sim 0.06 \pm 0.01$. We cannot rule out that imbrication may be formed during subcritical flows with ϕ values as low as 0.03, as demonstrated in a large number of flume experiments. However, our results from Alpine streams suggest that clast imbrication likely reflects upper flow regime conditions where clasts form well-sorted and densely packed clusters. We consider that these differences may be rooted in a misfit between the observational and experimental scales.

1 Introduction

Conglomerates, representing the coarse-grained spectrum of clastic sediments, bear key information about the provenance of the material (Matter, 1964), the sedimentary environments (Rust, 1978; Middleton and Trujillo, 1984), and the hydro-climatic conditions upon transport and deposition (Duller et al., 2012; D'Arcy et al., 2017). Conglomerates display the entire range of sedimentary structures, including a massive-bedded fabric, cross beds and horizontal stratifications. However, the most striking feature is clast imbrication (Fig. 1a), which refers to a depositional fabric where sediment particles of similar sizes overlap each other, similar to a run of toppled

dominoes (e.g., Pettijohn, 1957; Yagishita, 1997; Rust, 1984; Potsma and Roep, 1985; Todd, 1996). Imbrication may lead to armor development and the interlocking of clasts. As a consequence the search for possible controls on this fabric has received major attention in the literature (e.g., Bray and Church, 1980; Carling, 1981; Aberle and Nikora, 2006).

In the past decades, clast imbrication in streams has been considered to record high-stage flows (Rust, 1978; Miall, 1978; Sinclair and Jaffey, 2001). This could occur in the upper flow regime, where the flow velocity of a stream v exceeds the wave's celerity c (Allen, 1997), i.e., the speed of a wave on the water surface. The ratio v/c of these velocities has been referred to as the Froude number F where, in
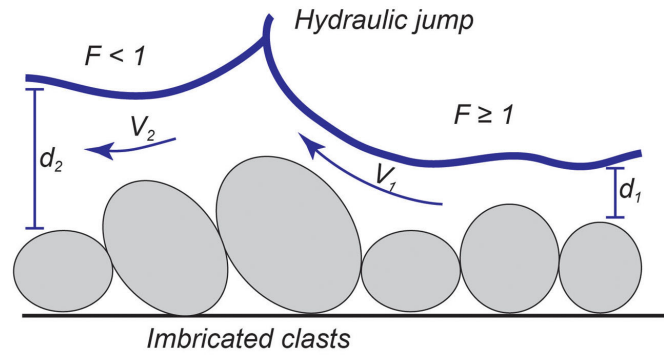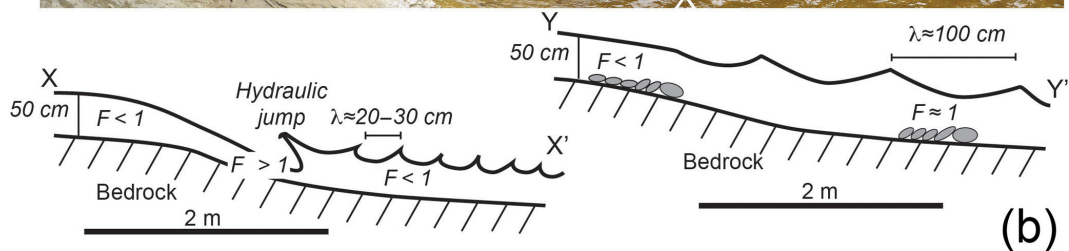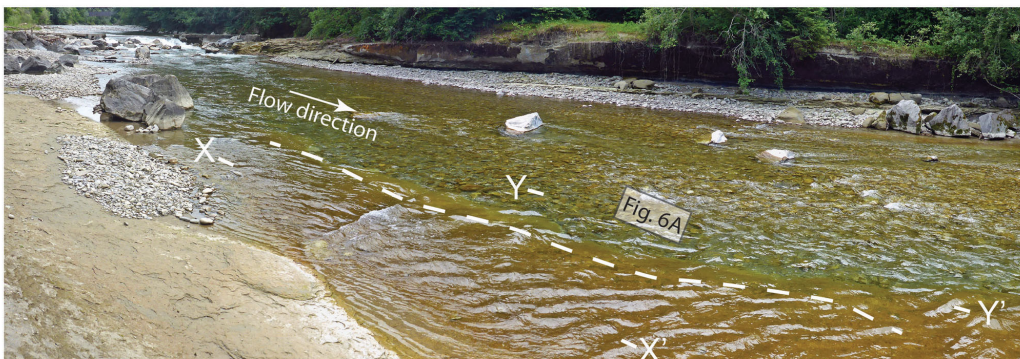
Figure 1. (a) Photo showing hydraulic jump, and conceptualization of the situation displayed in **(a)**. F is the Froude number; v is the flow velocity; d is the water depth. **(b)** Photo from Sense river, and cross sections through reaches with upper and lower flow regimes. Surface waves ($\lambda \approx 20$–30 cm) tend to fade out towards the upstream direction relative to the flow movement where subcritical flows prevail (section to the left). A hydraulic jump separates supercritical from subcritical flow where the bedrock builds a ramp. The reach illustrated by the section to the right is characterized by standing waves with wavelengths $\lambda \approx 100$ cm. The dashed line illustrates the trace of the plane that separates lower from upper regime flows. Please see Fig. 2 for location of photo.

theory, $F > 1$ denotes an upper flow regime or a supercritical flow, while $F < 1$ is characteristic for a lower flow regime or a subcritical flow (Engelund and Hansen, 1967). A hydraulic jump, which is characterized by a distinct increase in flow surface elevation and a decrease in flow velocity, marks the downstream transition from a super- to a subcritical flow (Fig. 1a). This hydrological condition is particularly mirrored by the surface texture in relation to water depth. Surface waves of subcritical flows have wavelengths that are smaller than water depths (Fig. 1b). The surface waves tend to migrate and fade out in the upstream direction with respect to the flow. Contrariwise, the wavelength of a standing wave, which is a feature of a supercritical flow ($F \approx 1$), is larger than water depth, and the surface wave is stationary (Supplement). Hydraulic jumps are manifested by a sudden decrease in the flow velocity and by an overturning of the flow surface (Fig. 1).

Significant sediment accumulation may occur underneath the hydraulic jump upon deceleration of the flow's velocity (Slootman et al., 2018). Contrariwise, a downstream change from a lower to an upper flow regime has no distinct surface expression, neither in terms of flow depth nor flow surface texture. While these mechanisms have been well explored and reported both from modern environments (e.g., Fig. 1) and fine-grained stratigraphic records (Alexander et al., 2001; Schlunegger et al., 2017; Slootman et al., 2018) and illustrated on photos from the field (Spreafacio et al., 2001), less evidence for a supercritical flow has been documented from conglomerates. This even led Grant (1997) to note that supercritical flows in fluvial channels are rare and that the use of the Froude number lacks justification from sedimentary records. In addition, Jarrett (1984) and Trieste (1992, 1994) considered that reports of inferred upper flow regimes might be biased by underestimations of the bed roughness in mountain streams. Nevertheless, the surface texture of the flow illustrated in Fig. 1a is characteristic for many streams (Spreafico et al., 2001), where hydraulic jumps are observed on the stoss side of large imbricated clasts. Furthermore, because the shift in large clasts such as cobbles and boulders does involve large shear stresses and thus high-discharge flows (Rust, 1978; Miall, 1978; Sinclair and Jaffey, 2001), the deposition of these particles, and particularly the formation of an imbricated fabric, is likely to occur during supercritical flows. Here, we explore the validity of this hypothesis for modern coarse-grained streams and stratigraphic records, and we calculate the related hydrological conditions. Similar to Grant (1997), we determine the Froude number at the incipient motion of coarse-grained bedload for various bed roughness and stream gradient values. We compare these results with data from modern streams in the Swiss Alps, stratigraphic records and published laboratory experiments.

2 Methods

2.1 Expressions relating flow regime to channel gradient and bed roughness

Channel depth and grain size are the simplest variables that can be extracted from stratigraphic records (Duller et al., 2012). These variables can additionally be used to calculate paleoslope and roughness values of streams for the geologic past (Paola and Mohring, 1996; Duller et al., 2012; Schlunegger and Norton, 2015; Garefalakis and Schlunegger; 2018), and they form the basis to related channel depth and grain size to flow strength and sediment transport. We therefore decided to focus on the simplest expressions that can also be applied to geological records. We are aware that this requires large generalizations and simplifications, which will not consider the entire range of hydrological complexities.

2.2 Boundary conditions

In the following, we consider the hydrological situation at the incipient motion of coarse-grained bedload. For these conditions, the dimensionless Shields parameter ϕ can be computed, which is the ratio between the shear stress exerted by the fluid on the bed τ_{cDi} at the onset of motion of a sediment particle with a distinct grain size D_i, as well as the inertial force of this grain (Shields, 1936; Paola et al., 1992; Paola and Mohring, 1996; Tucker and Slingerland, 1997):

$$\phi = \frac{\tau_{cDi}}{(\rho_s - \rho)g D_i}. \tag{1a}$$

Here, the constants ρ_s ($2700\,\mathrm{kg\,m^{-3}}$) and ρ denote the sediment and water densities, and g is the gravitational acceleration. The relationship expressed in Eq. (1a) predicts that a sediment particle with diameter D_i will be transported if the ratio between the fluid's shear stress τ_{cDi} and the particle's inertial force equals ϕ. Assignments of values to ϕ vary considerably and range between ca. 0.03 and 0.06, depending on the site-specific arrangement, the sorting and the interlocking of the clasts (Buffington and Montgomery, 1997; Church, 1978). This also includes the hiding and protrusion of small and large clasts, respectively, which exert a strong influence on the thresholds for clast entrainment (e.g., Egiazaroff, 1965; Parker et al., 1982; Andrews, 1984; Kirchner et al., 1990). Likewise, a smooth channel bed surface, such as a well-armored channel floor with well-sorted clasts, is likely to offer a greater resistance for the entrainment of a sediment particle than a gravel bar with poorly sorted material (Egiazaroff, 1965; Buffington and Montgomery, 1997).

The relationships denoted in Eq. (1a) differ for channel-forming floods, where channel-forming Shields stresses $\tau_{channel}$ are up to 1.2 times (Parker, 1978) above the threshold τ_{cDi} for the onset of grain motion. Pfeiffer et al. (2017) additionally showed that some rivers have a $\tau_{channel} / \tau_{cDi}$ ratio that is even higher. The consideration of channel-forming

floods thus requires larger thresholds:

$$\phi' \geq \frac{\tau_{\text{channel}}}{(\rho_s - \rho)g D_i} \approx 1.2 \frac{\tau_{\text{cDi}}}{(\rho_s - \rho)g D_i} = 1.2\phi. \quad (1b)$$

Accordingly, the critical shear stress τ_{cDi} for the entrainment of a sediment particle with a distinct grain size D_i can be computed through

$$\tau_{\text{cDi}} = \phi(\rho_s - \rho)g D_i. \quad (2)$$

Among the various grain sizes, the D_{84} has been considered as more representative for the gravel bar structure than the D_{50} (Howard, 1980; Hey and Thorne, 1986; Grant et al., 1990). In addition, the D_{84} has also been used for the quantification of the relative bed roughness, which is the ratio between grain size and water depth (e.g., Wiberg and Smith, 1991). If this inference is valid, then a major alteration of channel–bar arrangements requires a flow that is strong enough to entrain the D_{84} grain size.

A Shields variable of $\phi = 0.047$, which is based on flume experiments (Meyer-Peter and Müller, 1948) and observations in the field (Andrews, 1984), has conventionally been employed in a large number of studies (e.g., Paola and Mohring, 1996), particularly if the D_{50} is considered. Note that a reanalysis (Wong and Parker, 2006) of the Meyer-Peter and Müller (1948) data returned a value of $\phi = 0.0495 \approx 0.05$, which we employed in this paper. However, experiments also showed that material transport can occur at a lower threshold with a ϕ value as low as 0.03 (Ferguson, 2012; Powell et al., 2016). This might particularly be an appropriate threshold for the entrainment of the D_{84}, because of possible protrusion effects (e.g., Kirchner et al., 1990). Alternatively, Mueller et al. (2005) and Lamb et al. (2008) proposed that ϕ depends on channel gradient, where ϕ (for the D_{50} grain size) might exceed 0.1 for channels steeper than 1.1°. It appears that the threshold for the onset of grain motion varies depending on site and experiment-specific conditions. We therefore employed the entire range of ϕ values from 0.03 to 1.1 to comply with these complexities, which also includes channel-forming floods (Parker, 1978).

2.3 Hydrology, bed shear stress and onset of grain motion

Bed shear stress is calculated using an approximation for a steady, uniform flow down an inclined plane, where channel width is more than 20 times larger than water depth (e.g., Tucker and Slingerland, 1997):

$$\tau = g\rho S d. \quad (3)$$

Here, S denotes channel gradient, and d is water depth.

Alternatively, bed shear stress can also be computed as a function of the kinetic energy represented by the flow velocity v (Ferguson, 2007):

$$\tau = \frac{f}{8}\rho v^2. \quad (4)$$

The variable f, referred to as the Darcy–Weisbach friction factor (e.g., Papaevangelou et al., 2010), is a measure for the friction effect within the roughness layer at the flow bottom (Krogstad and Antonia, 1999). It also considers skin friction within the flow column (Ferguson, 2007). Ferguson (2007) reduced these complexities to a single expression, where f depends on water depth d relative to the grain size D_{84} and thus on the relative bed roughness:

$$\frac{f}{8} = \frac{\left(\frac{D_{84}}{d}\right)^2}{a_2^2} + \frac{\left(\frac{D_{84}}{d}\right)^{1/3}}{a_1^2}. \quad (5)$$

Here, a_1 and a_2 are constants that vary between 7–8 and 1–4, respectively (Ferguson, 2007), which have been calibrated to $a_1 = 7.5$ and $a_2 = 2.36$ (Ferguson, 2007). We additionally considered possible consequences of energy loss through assignments of different values to the Shields (1936) variable (see explanation of Eq. 1a above). We are aware that we could also employ Manning's number n for the characterization of the channel's fabric (Whipple, 2004) and the relative bed roughness (Jarrett, 1984). Related expressions (Jarrett, 1984) predict that n hinges on channel gradient and water depth only and not on bed structure. We thus prefer to use Ferguson's (2007) approach (Eq. 5), which explicitly considers the relative bed roughness, consistent with the most recent work by Wickert and Schildgen (2018, see their Eq. 13).

As outlined in the introduction, the Froude number F depends on the ratio of flow velocity v and surface wave celerity c. For shallow waters, which is commonly the case for rivers and streams, this relationship can be computed if water depth d is known:

$$F = \frac{v}{c} = \frac{v}{\sqrt{gd}}. \quad (6)$$

The combination of Eqs. (3), (4) and (6) then yields a simple expression where

$$F = \sqrt{8\frac{S}{f}}. \quad (7)$$

This expression states that the Froude number F depends on two partly unrelated variables. In particular, for a given bed friction f, an upper flow regime tends to establish for steep channels. Contrariwise, a lower regime is maintained where poorly sorted material exerts a large resistance on the flow, thereby reducing the flow velocity and hence the Froude number. Accordingly, the dependency of F on channel gradient S can be computed through the combination of Eqs. (2), (3), (5) and (7):

$$F = \sqrt{\frac{S}{\left(\frac{\rho S}{\phi(\rho_s - \rho)}\right)^2 \cdot a_2^{-2} + \left(\frac{\rho S}{\phi(\rho_s - \rho)}\right)^{1/3} \cdot a_1^{-2}}}. \quad (8)$$

Alternatively, an expression where the Froude number depends on the bed roughness D_{84}/d only can be achieved
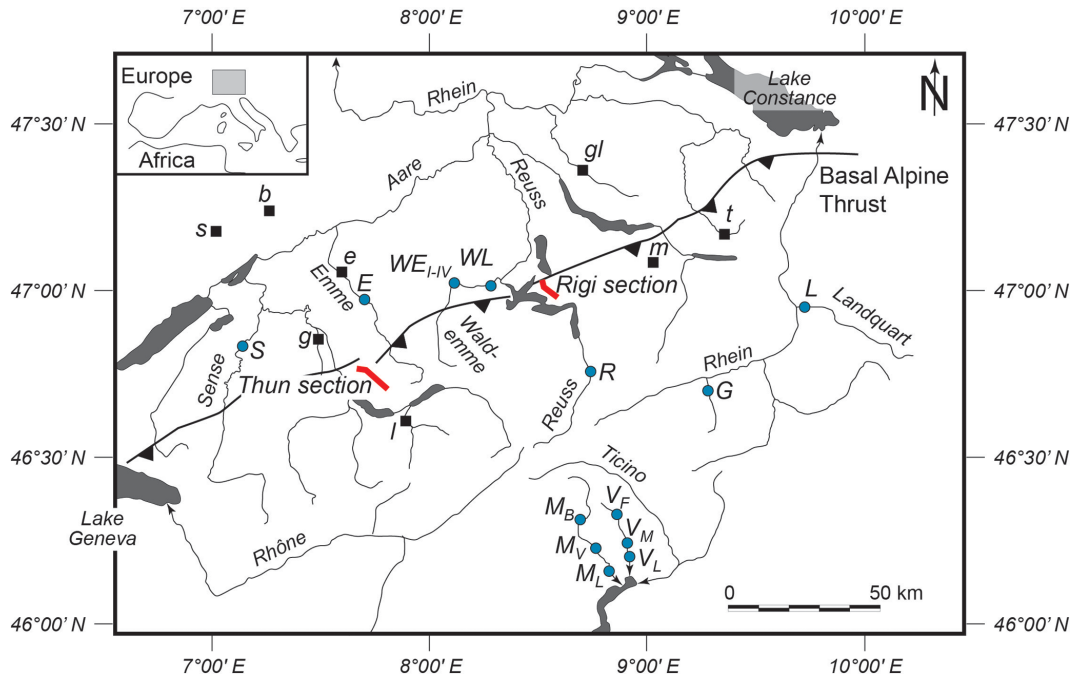
Figure 2. Sites where modern gravel bars in streams were inspected for the occurrence of clast imbrication (blue dots). The figure also shows the locations of the stratigraphic sections where conglomerates were analyzed for their sedimentary structures. S: Sense; E: Emme; WE_{I-IV}: Waldemme; WL: Waldemme at Littau; R: Reuss; L: Landquart; G: Glenner; M_B, M_V and M_L: Maggia at Bignasco, Visletto and Losone; V_F, V_M and V_L: Verzasca at Frasco, Motta and Lavertezzo. See Table 1 for coordinates of sites. The black squares are sites where Spreafico et al. (2001) have estimated channel gradients and Froude numbers for low- and high-stage flows. b: Birse-Moutier, e: Emme-Burgdorf, gl: Glatt-Fällanden, g: Gürbe-Belp, m: Minster-Euthal, l: Lütschine-Gsteig, s: Suze-Sonceboz, t: Thur-Stein.

through the combination of equations 2, 3 and 7:

$$F = \sqrt{8 \cdot \frac{\phi(\rho_s - \rho)}{\rho \cdot f} \cdot \frac{D_{84}}{d}}. \tag{9}$$

We thus used Eqs. (8) and (9) to calculate the Froude numbers at the onset of motion of the D_{84} grain size. We then compared these results with data from modern streams and stratigraphic records.

2.4 Collection of data from modern streams and stratigraphic records

We used observations about clast arrangements in gravelly streams in Switzerland. We paid special attention to the occurrence of clast imbrication, as we hypothesize that this fabric may document the occurrence of an upper flow regime (Fig. 1) upon sedimentation and gravel bar migration. We explored multiple gravel bars for the occurrence or absence of clast imbrication over a reach of several hundreds of meters where Litty and Schlunegger (2017) reported grain size data (Table 1). We then determined a mean energy gradient over a ca. 500 m long reach, which we calculated from topographic maps at scales 1 : 10 000.

The selected streams are all situated around the Central Alps (Fig. 2), have different source rock lithologies (Spicher,

1980) and have different grain size distributions. At sites where grain size data have been collected, the ratio between the clasts' medium b and longest a axes is constant and ranges between 0.67 and 0.72, irrespective of the grain size distribution in these streams (Litty and Schlunegger, 2017). For these sites, we calculated the bed roughness D_{84}/d at the incipient motion of the D_{84}. Here, related water depths d were determined through the combination of Eqs. (2) and (3) and using the channel gradient S at these sites.

The Swiss Federal Office for the Environment (FOEN) estimated the Froude numbers for various flood magnitudes of streams on the northern side of the Swiss Alps (Spreafico et al., 2001; see Fig. 2 for location of sites). These estimates are based on flow velocities, flow depths and cross-sectional geometries of channels. The authors of this study also determined the corresponding channel gradient over a reach of several hundred meters. We will thus use the Spreafico et al. (2001) dataset to constrain the range of possible ϕ values for streams in Switzerland.

We finally identified relationships between channel gradient, bed roughness and clast imbrication from stratigraphic records. We focused on the late Oligocene suite of alluvial megafan conglomerates (Rigi and Thun sections, Fig. 2) deposited at the proximal border of the Swiss Molasse basin. For these conglomerates, Garefalakis and Schluneg-

Table 1. Grain size and observational data and that have been collected in the field. See text for further explanations.

Site name / Segment	Abbreviation	Site coordinates	D_{84} (cm) / (m)	D_{50} (cm)	D_{84}/D_{50}	D_{96} (cm)	Gradient / Slope (mm^{-1})	Gradient / Slope (°)	Inferred water depth d (m)	Roughness / D_{84}/d	Imbrication
Modern gravel bars											
Emme	E	46°57′08″ N, 7°44′59″ E	2.3	0.9	2.56	5.2	0.005–0.008	0.4 ± 0.1	0.5–0.8	0.07–0.10	mostly no
Glenner	G	46°44′42″ N, 9°13′04″ E	12	2.88	4.17	27.4	0.017–0.024	1.2 ± 0.2	0.4–0.6	0.22–0.31	mostly yes; largest boulders imbricated
Landquart	L	46°57′08″ N, 7°44′59″ E	10	2.5	4.00	13.5	0.014–0.021	1.0 ± 0.2	0.4–0.6	0.18–0.27	yes
Maggia Bignasco	MB	46°44′42″ N, 9°13′04″ E	2.7	0.85	3.18	13	0.009–0.012	0.6 ± 0.1	0.2	0.12–0.16	mostly no, but triplets of imbricated clasts occur in places as inferred from photos
Maggia Visletto	MV	46°58′26″ N, 9°36′29″ E	9.5	2.29	4.15	20	0.009–0.012	0.6 ± 0.1	0.3–0.5	0.12–0.16	partly yes
Maggia Losone I	ML I	46°20′08″ N, 8°36′25″ E	4	0.79	5.06	14	0.005–0.007	0.3 ± 0.1	0.5–0.6	0.07–0.09	triplets and quadruplets of imbricated clasts occur in places
Maggia Losone II	ML II	46°18′30″ N, 8°36′35″ E	6	1.12	5.36	12.65	0.005–0.007	0.3 ± 0.1	0.7–1.0	0.07–0.09	triplets and quadruplets of imbricated clasts occur in places
Verzasca Frasco	VF	46°10′46″ N, 8°45′33″ E	2.5	0.75	3.33	7	0.015–0.026	1.3 ± 0.2	0.1	0.20–0.34	imbricated
Verzasca Motta	VM	46°10′15″ N, 8°46′10″ E	4.3	1.44	2.99	18.75	0.012–0.016	0.9 ± 0.2	0.2–0.3	0.16–0.21	largest boulders imbricated, smaller pebbles deposited in-between without preferred orientation, finer-grained bedforms show imbricated clasts where no boulders are present
Verzasca Lavartezzo	LV	46°20′20″ N, 8°48′03″ E	5	1.3	3.85	30	0.016–0.023	1.1 ± 0.2	0.2–0.3	0.21–0.30	largest boulders imbricated, smaller pebbles deposited in-between without orientation as inferred from photos
Reuss		46°16′28″ N, 8°48′34″ E	3.2	0.88	3.64	6.37	0.005–0.008	0.4 ± 0.1	0.3–0.5	0.07–0.10	to large extents yes, triplets and quadruplets of imbricated clasts occur in places
Sense		46°1′21″ N, 8°50′23″ E	6	2.42	2.48	9.58	0.005–0.007	0.3 ± 0.1	0.7–1.0	0.07–0.09	shows standing waves and hydraulic jumps in steep reaches and lower flow regime conditions in flat segments
Stratigraphic archives											
Rigi conglomerates — Segment	Abbreviation	Site coordinates	D_{84} (m)				Slope (mm^{-1})	Slope (°)	Inferred water depth d (m)	D_{84}/d	Imbrication
Waldemme Litau	WL	46°48′53″ N, 8°39′16″ E	3.5	0.9	3.89	8.36	0.009–0.012	0.6 ± 0.1	0.2–0.3	0.12–0.16	mostly no; imbrication only at the steep downstream slip faces of transverse bars
Waldemme Entlebuch I	WE I	46°53′20″ N, 7°20′56″ E	3	1	3.00	9	0.01–0.017	0.8 ± 0.2	0.1–0.2	0.13–0.22	triplets and quadruplets of imbricated clasts occur in places
Waldemme Entlebuch II	WE II	47°03′04″ N, 8°15′13″ E	8	2.43	3.29	18	0.01–0.017	0.8 ± 0.2	0.4–0.6	0.13–0.22	yes
Waldemme Entlebuch III	WE III	47°01′57″ N, 8°04′03″ E	5.7	2.57	2.22	14	0.01–0.017	0.8 ± 0.2	0.3–0.5	0.13–0.22	yes
Waldemme Entlebuch IV	WE IV	47°01′57″ N, 8°04′03″ E	8.2	2.68	3.06	18	0.01–0.017	0.8 ± 0.2	0.4–0.7	0.13–0.22	yes
Thun conglomerates — Segment			D_{84} (m)				Slope (mm^{-1})	Slope (°)	Inferred water depth d (m)	D_{84}/d	Imbrication
δ			0.07–0.12				0.009–0.027	0.9 ± 0.4	1.2 ± 0.35	0.05–0.14	yes, in places
γ			0.06–0.1				0.008–0.015	0.65 ± 0.2	1.2 ± 0.4	0.04–0.12	partly yes
β			0.04–0.06				0.005–0.01	0.4 ± 0.2	1.7 ± 0.5	0.02–0.05	no
α			0.04–0.06				0.002–0.005	0.2 ± 0.06	2.5 ± 0.8	0.02–0.04	no
B			not available				0.008–0.017	0.72 ± 0.3	1.5–3	not available	yes, in places
A			not available				0.003–0.005	0.23 ± 0.1	3–5	not available	no

ger (2018) and Schlunegger and Norton (2015) collected data about the depth and gradient of paleochannels, as well as information about the grain size distribution along ca. 3000 to 3600 m thick sections (Table 1). We returned to these sections and examined ca. 50 sites for the occurrence of clast imbrication within the conglomerate suites.

3 Results

3.1 Calculation of flow regime as a function of bed roughness and channel gradient

We calculated the Froude numbers F for different channel gradient S and bed roughness D_{84}/d values, as well as thresholds ϕ for the incipient motion of material. We compared these results with observations from modern streams and stratigraphic records. We avoided calculation of the Froude numbers for slopes steeper than 1.4° because channels tend to adapt a step-pool geometry in their thalwegs (Whipple, 2014), for which our calculations no longer apply. We set the thresholds for a critical flow to a Froude number $F = 0.9$, which is consistent with estimations for the formation of upper flow regime bedforms by Koster (1978). Calculations were initially carried out using $\phi = 0.0495 \approx 0.05$, as this value has commonly been used in a large number of studies (see above). The results reveal that F increases with steeper channels (Fig. 3a) and reaches the field of a critical flow for $\sim 0.5°$ slopes. The values reach a maximum of $F \approx 1$ where channel gradients are between ~ 0.8 and 1°. Froude numbers F then slightly decrease for channels steeper than 1° and finally reach a value of 0.9 for gradients $> 1.2°$. In the case of a greater threshold for the onset of grain motion, expressed through $\phi = 0.06$, flows adapt supercritical conditions for channels steeper than $\sim 0.4°$. For a lower threshold, expressed here through $\phi = 0.03$, streams remain in the lower flow regime.

The Froude number pattern is quite similar for increasing bed roughness (Fig. 3b). For $\phi = 0.0495 \approx 0.05$ the Froude numbers increase with higher relative bed roughness. Supercritical conditions are reached for a bed roughness of ca. 0.1, after which the Froude numbers decrease with larger roughness. For $\phi = 0.06$ an upper flow regime might prevail for bed surface roughness values between 0.06 and 0.5. Smaller and larger roughness values will keep the flow in the lower regime. Contrariwise, the flow will not shift to the upper regime for ϕ values as low as 0.03. Note that the consideration of the full range of roughness layer and skin friction effects, expressed through the coefficients a_1 and a_2 in Eq. (8), shifts the pattern of Froude numbers to lower and higher values. But this will not alter the general finding that at the onset of grain motion an upper flow regime is expected (i) for a channel gradient S steeper than 0.5° ± 0.1° and (ii) for a bed roughness D_{84}/d greater than ~ 0.06.

We also calculated the Froude numbers for $\phi = 0.1$, because observations have shown that thresholds for the en-

trainment of sediment particles increase with steeper channels (Mueller et al., 2005; Ferguson, 2012). This might be an exaggeration (Lamb et al., 2008), but will give an upper bound for the dependence of the Froude number F on the Shields variable ϕ. We additionally considered the case where ϕ depends on S through $\phi = 2.81 \cdot S + 0.021$ (Mueller et al., 2005). These relationships have been established based on bedload rating curves for mountain streams in North America and England. We found that the flows shift to critical conditions for channels steeper than between 0.5° and 0.6° (slope dependent ϕ) and for a bed roughness > 0.04 ($\phi = 0.1$).

In summary, the calculations predict that water flow may shift to an upper flow regime for

(i) ϕ values greater than 0.05,

(ii) slopes steeper than $\sim 0.5° \pm 0.1°$ and

(iii) relative bed roughness values greater than $\sim 0.06 \pm 0.01$.

3.2 Estimates of φ values from modern streams in the Central Alps

Spreafico et al. (2001) estimated the Froude numbers for various streams situated on the northern side of the Swiss Alps. The F values range between 0.2 and 1.1 and generally increase with channel gradients (vertical bars on Fig. 3a). The flow's surfaces particularly of the Birse and Thur streams (labeled as b and t on Fig. 3a) are characterized by multiple hydraulic jumps (Spreafico et al., 2001, p. 71 and p. 77). Therefore, the inferred small Froude numbers (between 0.6 and 0.9) of these streams have to be treated with caution.

The Froude number estimates by Spreafico et al. (2001) disclose a large scatter in the relationship to channel gradient (Fig. 3a, vertical bars). This can partially be explained by site-specific differences in bed roughness due to anthropogenic corrections and constructions (Spreafico et al., 2001). Nevertheless, the comparison between these data and the results of our calculations reveal that the entire range of ϕ values between 0.03 and 0.1 has to be taken into account for the hydrological conditions in the streams surrounding the Swiss Alps (Fig. 3a). This also implies that the selection of a threshold, expressed by the ϕ value, warrants a careful justification, which we present in the discussion.

3.3 Occurrence or absence of clast imbrication in modern streams

Here, we present evidence for imbrication and non-imbrication from modern rivers situated both in the core of the Swiss Alps and the foreland, which we relate to channel slope (Fig. 4a) and bed roughness (Fig. 4b). The bedrock geology of the headwaters includes the entire range of lithologies from sedimentary units to schists, gneisses and granites.
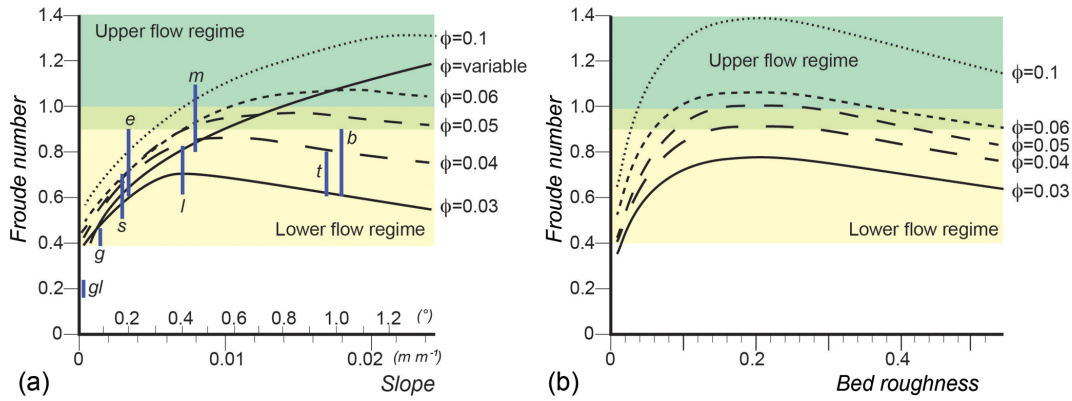
Figure 3. Relationships between **(a)** channel slope and Froude number F and **(b)** relative bed roughness and F. These were calculated as a function of various Shields (1936) variables ϕ. The pale green field indicates the conditions where an upper flow regime could prevail, while the yellow field delineates the occurrence of lower flow regime conditions. In this context, we set the threshold to a Froude number of ca. 0.9. This is consistent with the estimation of parameters for the formation of upper flow regime bedforms by Koster (1978). Note that the bed roughness is the ratio between the D_{84} and the water depth d at the onset of motion of that particular size class. The vertical bars on **(a)** also illustrate the Froude numbers that have been estimated by Spreafico et al. (2001) for the following streams and locations. b: Birse-Moutier, e: Emme-Burgdorf, gl: Glatt-Fällanden, g: Gürbe-Belp, m: Minster-Euthal, l: Lütschine-Gsteig, s: Suze-Sonceboz, t: Thur-Stein. Please note that the low values for the Thur and Birse rivers might represent underestimates as these streams show evidence for multiple hydraulic jumps during high-stage flows.
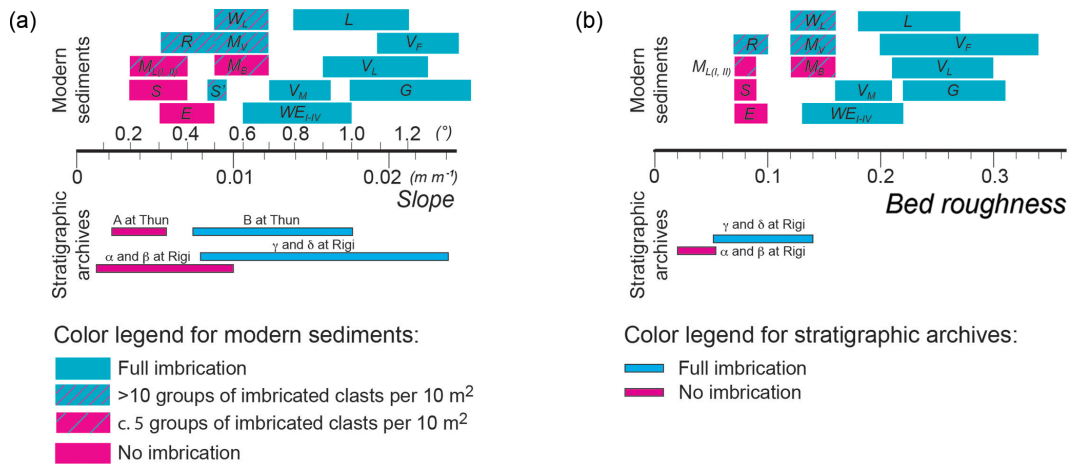

Figure 4. This figure relates the occurrence of imbrication (blue bars) or no imbrication (red bars) to **(a)** channel slopes and **(b)** relative bed roughness. Red bars with blue hatches indicate that imbrication has been found in places. Blue bars with red hatches suggest that imbrication dominates the bar morphology, but that reaches without imbrication are also present on the same gravel bar. Data from modern streams are displayed above the horizontal axes, while information from stratigraphic sections are placed below the slope and roughness axes, respectively. S: Sense; S': Sense with bedrock reach; E: Emme; WE_{I-IV}: Waldemme; WL: Waldemme at Littau; R: Reuss; L: Landquart; G: Glenner; M_B, M_V and M_L: Maggia at Bignasco, Visletto and Losone; V_F, V_M and V_L: Verzasca at Frasco, Motta and Lavertezzo. See Table 1 for coordinates of sites and Fig. 2 for locations where data were collected.

In addition, the streams cover the full range of water sources including glaciers and surface runoff. Except for the Maggia river between the sites Bignasco and Losone (Fig. 2), all streams are channelized by artificial riverbanks. These are either made up of concrete walls or outsized boulders. Information about the hydrographs, grain size and the results of the shear stress calculations considers the time after these constructions have been made.

3.3.1 Channel morphologies

The thalweg of the streams meanders between the artificial walls within a 20 to 50 m wide belt. Flat-topped longitudinal bars that are several tens of meters long and that emerge up to 1.5 m above the thalweg are situated adjacent to the artificial riverbanks on the slip-off slope of these meanders. They evolve into subaquatic transverse bars, or riffles, farther downstream where the thalweg shifts to the opposite

channel margin. Channels are deepest and flattest along the outer cutbank side of the meanders and in pools downstream of riffles, respectively. The thalweg then steepens where it crosses the transverse bars and riffles. This is also the location where some streams show evidence for standing waves with wavelengths >5 m (e.g., at Reuss, Fig. 5). Standing waves have also been encountered in the Waldemme river at Littau (Fig. 6b; see supplement) when water runoff at that particular site was ca. $100 \, \text{m}^3 \, \text{s}^{-1}$ and when rumbling sounds indicated that clasts were rolling or sliding. The streams thus display a complex pattern where channel depths, flow velocities and hydrological regimes alternate over short distances of tens to hundreds of meters. These arrangements of channel–bar pairs and particularly their positions within the channel belt have been stable over the past years because the gravel bars are situated in the same locations as the ones reported by Litty and Schlunegger (2017).

3.3.2 Streams with evidence for clast imbrication

Inspections of gravel bars have shown clear evidence for imbrication in the Glenner, the Landquart, the Verzasca and the Waldemme rivers (Table 1). In these streams, channel gradients range between 0.6° (Waldemme) and 1.2° (Glenner) (Fig. 4a). The sizes of the D_{84} range between 3 cm (Waldemme) and 12 cm (Glenner). The gravel lithology includes the entire variety from sedimentary (Waldemme) to crystalline constituents (Glenner, Landquart, Verzasca). The inferred bed roughness at the onset of motion of the D_{84} includes the range between ca. 0.125 (Waldemme) and 0.31 (Glenner) (Fig. 4b). In these streams, bars with imbricated clasts alternate with pools over a reach of several hundreds of meters.

At Maggia, Reuss and Waldemme Littau, the largest clasts are arranged as triplets or quadruplets of imbricated constituents within generally flat-lying to randomly oriented finer-grained sediment particles. The density of these arrangements ranges between 5 groups per $10 \, \text{m}^2$ (Maggia Bignasco, Maggia Losone) to ca. 10 groups per $10 \, \text{m}^2$ (Maggia Visletto, Reuss, Waldemme Littau; e.g., Fig. 6d). The channel gradients at these sites span the range between ca. 0.3 and 0.6°, and the D_{84} clasts are between 3 and 9 cm large (Reuss and Maggia Visletto). Accordingly, the relative bed roughness at the incipient motion of the D_{84} ranges between 0.07 and 0.16.

At all sites mentioned above, clasts on subaquatic and subaerial gravel bars are generally arranged as well-sorted and densely packed clusters, possibly representing incipient bedforms (e.g., Fig. 6d). In most cases, grains imbricate behind an outsized clast, which usually delineates the front of imbricated grains. In addition, the lowermost 10 % to 20 % part of most of the large clasts is embedded, and thus buried, in a fine-grained matrix, which was most likely deposited during the waning stage of a flood. Isolated, unburied clasts that are flat lying on their a–b planes are less frequent than embedded
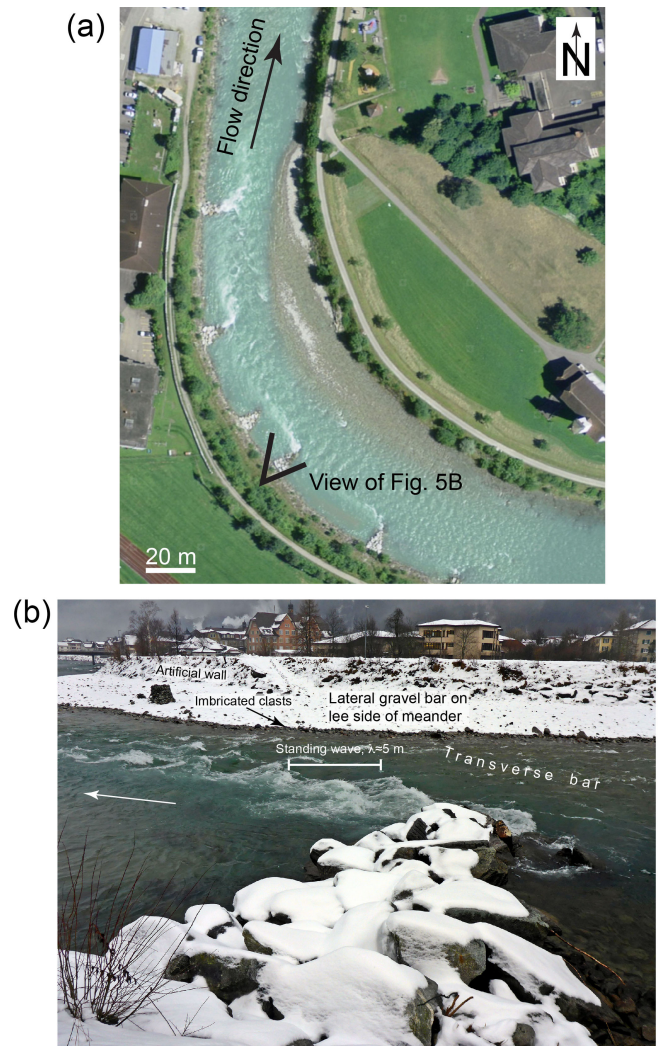

Figure 5. **(a)** Reuss river with evidence for standing waves along the thalweg. Orthophoto reproduced with the permission of swisstopo (BA 18065). Please see Fig. 2 for location. **(b)** Transverse and lateral bars in the Reuss river with imbricated clasts on the lateral bar forming a riffle, and standing waves where the thalweg crosses the riffle. The wavelength of the standing wave is ca. 5 m. Arrow indicates flow direction. Please see Figs. 2 and 5a for location of photo.

clasts or constituents arranged in clusters. The inclination dip of the a–b planes ranges between ca. 20° to 40° (Fig. 6d). Finally, streams with clast imbrications display surface expressions, which point to an upper flow regime during low- (e.g., Reuss, Fig. 5b) and high-water stages (e.g., Waldemme, Fig. 6b, see Supplement).

3.3.3 Streams with little or no evidence for clast imbrication

Gravel bars within the Emme stream are made up of generally flat-lying gravels and cobbles. A small tilt (< 10°) of a–
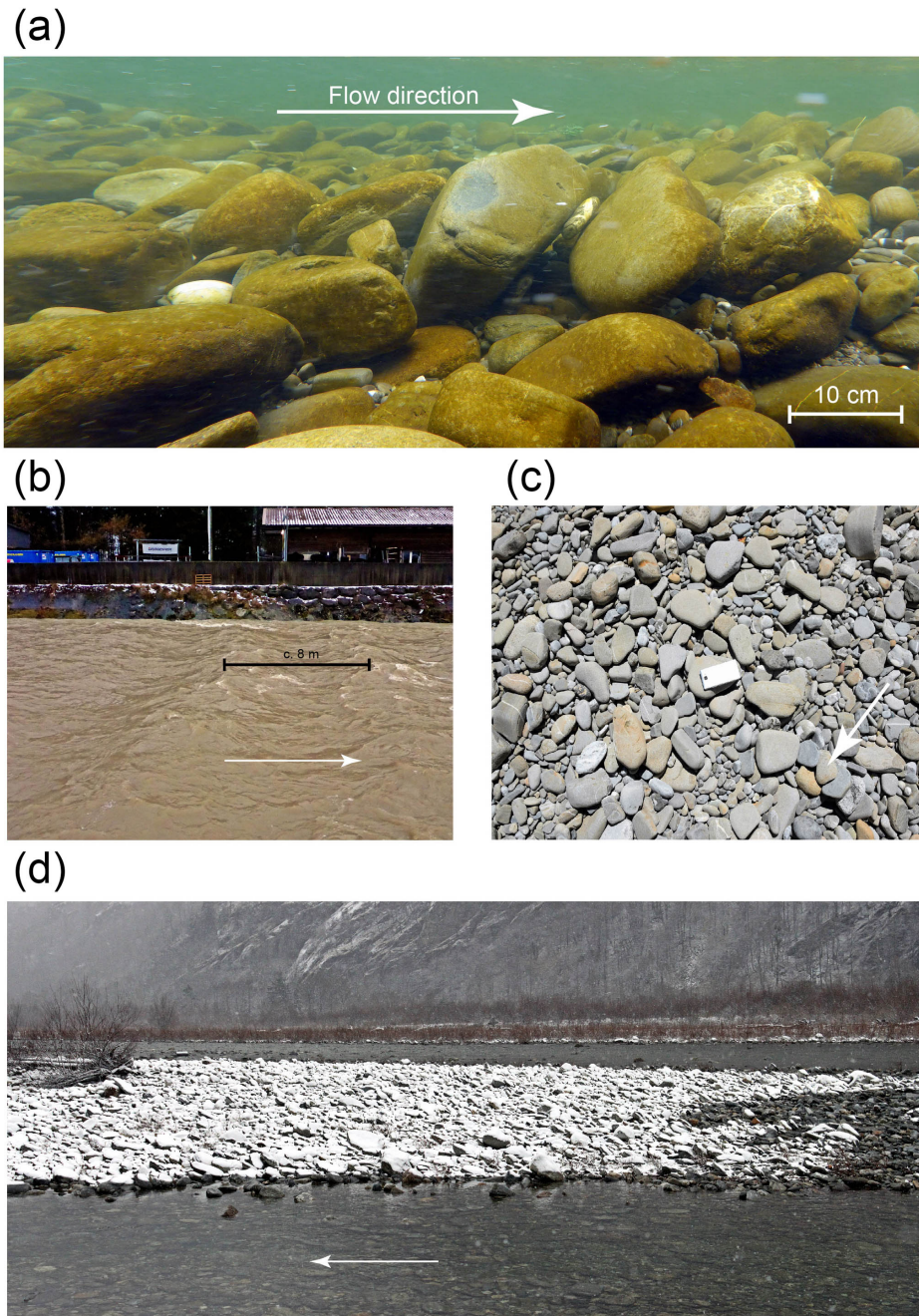
Figure 6. Photos from the field. **(a)** Photo of a subaquatic longitudinal bar taken along the steep bedrock/gravel bar reach of the Sense river (see Fig. 1b for location of photo). The clasts in the foreground are clustered and imbricated, forming the nucleus of a possible cluster bedform. This fabric most likely formed when rolling clasts came to a halt behind the boulder at the front. The clasts in the background are either flat lying or slightly imbricated. Except for a few sites, nearly all grains are either partially buried by finer-grained material or interlocked by neighboring clasts. The overlying flow shows evidence for supercritical conditions with standing waves. **(b)** Standing waves with a wavelength of ca. 8 m in the Waldemme at Littau. Water fluxes are ca. $100 \, \text{m}^3 \, \text{s}^{-1}$. Arrow indicates flow direction. See also supplement. **(c)** Flat-lying clasts on a lateral bar in the Sense river. Arrow indicates clasts that are overlapping each other, resulting in a shallow dip of <10° of the overriding clast. **(d)** Imbricated clasts within the Maggia river at Visletto. Arrow indicates flow direction. Please note that the imbricated arrangements of clasts mainly include the largest constituents of the gravel bar in the middle of the photo and clasts of similar sizes. Therefore, for this set of imbricated clasts, we do not consider that protrusion effects might play a major role. See Fig. 2 for location and Table 1 for coordinates.
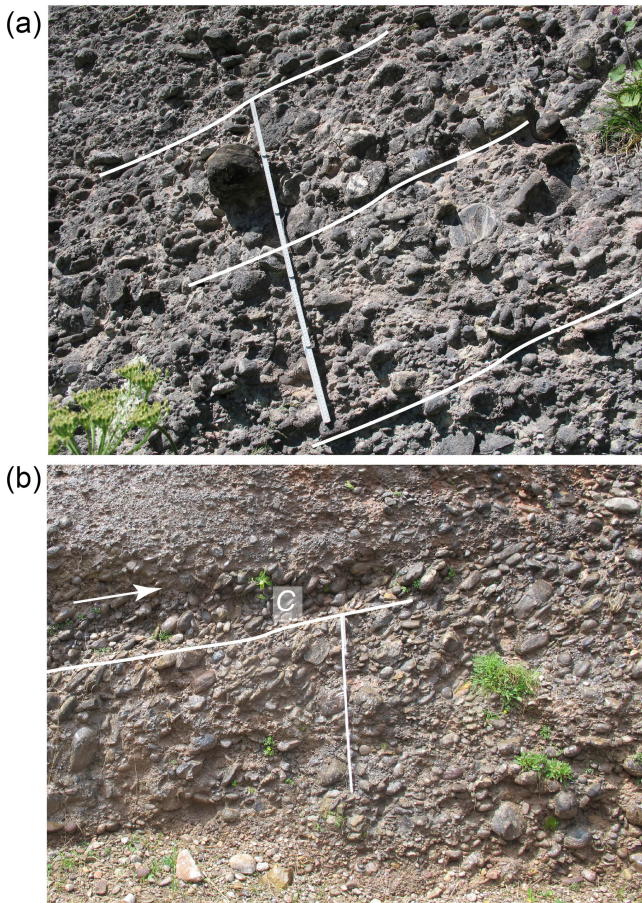
Figure 7. (a) Conglomerates at Rigi with no evidence for clast imbrication. White lines indicate the orientation of the bedding. (b) Conglomerates at Rigi with imbricated gravels to cobbles that are arranged as cluster bedforms (C). Arrow indicates paleoflow direction. White line refers to the bedding. Note the steep dip ($> 25°$) of the a–b planes of the imbricated clasts. See Fig. 2 for location and Table 1 for coordinates.

b planes occurs where individual clasts slightly overlap each other, similar to a shingling arrangement of particles. This is particularly the case in pools and on the upstream stoss side of longitudinal and transverse bars where channel gradients are flat. Also in the Emme river, clast imbrication occurs in places only where gravel bars have steep downstream slip faces, which are mainly observed at the end of transverse bars. At sites where imbrication is absent, most of the clasts are lying flat on their a–b planes, and embedding by finer-grained material is less frequently observed than in streams with clast imbrication. The channel gradient is less than $0.5°$, and the size of the D_{84} measures 2 cm. The bed roughness of this stream, calculated for the incipient motion of the 84th grain size percentile, ranges between 0.07 and 0.10. Finally, the flow has a smooth surface during low- and high-water stages (Spreafico et al., 2001, p. 53), which points to a lower flow regime.

The Sense river differs from the Emme stream in the sense that bedrock reaches alternate with alluvial segments over 100–200 m and more. Alluvial segments are flat (ca. $0.3°$) and host lateral and transverse gravel bars where the D_{84} measures 6 cm. On top of these bars, gravels generally rest flat on their a–b planes (Fig. 6c). Imbrication is observed where some of these gravels overlap each other, resulting in a dip angle of 10–$20°$. Contrariwise, bedrock reaches (site S' on Fig. 4a) that form distinct steps in the thalweg are up to $0.5°$ steep and partly covered by subaquatic longitudinal bars (Fig. 1b) where imbricated clasts alternate with flat-lying grains at the meter scale. The channel bed surface is generally well sorted and well armored. Clasts are either interlocked, partly isolated or also rooted in a finer-grained matrix (Fig. 6a). At these sites, upper flow regime segments laterally change to lower flow regime reaches over short distances of a few meters (Fig. 1b). While we have made this observation during low-water stages only, it is likely that sub- and supercritical flows also change during flood stages over short distances, as various examples of Alpine streams show (Spreafico et al., 2001).

3.4 Data about clast imbrication from stratigraphic records

Here, we calculated patterns of bed roughness and related channel gradients from stratigraphic records and explored ca. 50 conglomerate sites for clast imbrication. We used published data about channel depth d, surface gradient S and information about the pattern of the D_{84}, which have been reported from the late Oligocene alluvial megafan conglomerates at Rigi ($47°03'$ N, $8°29'$ E) and Thun ($46°46'$ N, $7°44'$ E) situated in the Molasse foreland basin north of the Alpine orogen (Fig. 2, Table 1). The depositional evolution of these conglomerates has been related to the rise and the erosion of the Alpine mountain belt (Kempf et al., 1999; Schlunegger and Castelltort, 2016).

The Rigi deposits are ca. 3600 m thick and made up of an alternation of conglomerates and mudstones (Stürm, 1973) that were deposited between 30 and 25 Ma according to magneto-polarity chronologies and mammal biostratigraphic data (Engesser and Kälin, 2017). Garefalakis and Schlunegger (2018) subdivided the Rigi section into four segments labeled as α through δ. The lowermost segments α and β are an alternation of mudstones and conglomerate beds and were deposited by gravelly streams (Stürm, 1973). According to Garefalakis and Schlunegger (2018), the depositional area was characterized by a low surface slope between $0.2 \pm 0.06°$ and $0.4 \pm 0.2°$. Channel depths span the range between 1.7 and 2.5 m, and the D_{84} values are between 2 and 6 cm. These measurements result in bed roughness values between 0.02 and 0.05. Except for one site, we found no evidence for imbrication in α and β units (Figs. 4, 7a).

The top of the Rigi section, referred to as segments γ and δ by Garefalakis and Schlunegger (2018), is an amal-

gamated stack of conglomerate beds deposited by non-confined braided streams (Stürm, 1973). Garefalakis and Schlunegger (2018) inferred values between $0.65° \pm 0.2°$ and $0.9° \pm 0.4°$ for the paleogradient of the river (Table 1). D_{84} values range between 6 and 12 cm, and paleochannels were ca. 1.2 m deep. This yields a relative bed roughness between ca. 0.05 and 0.12. Interestingly, a large number of conglomerate sites within γ and δ display evidence for clast imbrication in outcrops parallel to the paleodischarge direction (Figs. 4, 6b). In addition, some outcrops show sedimentary structures that correspond to cluster bedforms of imbricated clasts (C on Fig. 7b). However, at all sites, the lateral extent of these bedforms is limited to 1–2 m. Please refer to Garefalakis and Schlunegger (2018) and their Fig. 2 for location of sites displaying units α through δ.

The ages of the up to 3000 m thick Thun conglomerates are younger and span the time interval between ca. 26 and 24 Ma according to magneto-polarity chronologies (Schlunegger et al., 1996). Similar to the Rigi section, the Thun conglomerates start with an alternation of conglomerates, mudstones and sandstones (unit A). This suite is overlain by an up to 2000 m thick amalgamated stack of conglomerate beds (unit B). Channel depths within unit A range between 3 and 5 m, and streams were between 0.1° and 0.3° steep. Channels in the overlying unit B were shallower and between 1.5 and 3 m deep. Stream gradients varied between 0.4° and 1°, depending on the relationships between inferred water depths and maximum clast sizes (Schlunegger and Norton, 2015). In outcrops parallel to the paleodischarge direction, sequences with imbricated clasts have only been found in unit B where paleochannel slopes were steeper than 0.4° (Fig. 4a). Similar to the Rigi section, the lateral extents of imbricated clasts are limited to a few meters only. No data are available for computing the D_{84} grain size, so that we cannot estimate the bed roughness for the Thun conglomerates. Please refer to Schlunegger and Norton (2015) for location of sites where units A and B are exposed.

Similar to the modern examples, imbricated clasts form a well-sorted cluster and commonly include the largest constituents of a gravel bar. In most cases, clasts imbricate behind an outsized constituent, which usually delineates the front of imbricated grains (Fig. 7b).

4   Discussion

4.1   Selection of preferred boundary conditions

Our calculations reveal that the results are strongly dependent on the following:

i.   The selection of values for the Shields variable ϕ.

ii. The way in which we consider variations in slope S at the bar and reach scales.

iii. The consideration of flood magnitudes which either result in the motion of individual sediment particles or the change in an entire channel (channel-forming floods).

This section is devoted to justify the selection of our preferred boundary conditions.

4.1.1   Channel-forming floods versus onset of grain motion and related thresholds

We constrained our calculations on the incipient motion of individual clasts and used Eq. (1a) for all other considerations. This might contrast to the hydrological conditions during channel-forming floods where thresholds for the evacuation of sediment are up to 1.2 times larger, as theoretical and field-based analyses and have shown (Parker, 1978; Philips and Jerolmack, 2016; Pfeiffer et al., 2017). However, a 1.2-times larger threshold will increase the ϕ values (Eq. 1b) to the range between 0.036 and 0.072. As illustrated in Fig. 3, this will not change the general pattern. In addition, while channel-forming floods mainly result in the shift of a large range of sediment particles, the formation of an imbricated fabric involves the clustering of individual clasts only. We use these arguments to justify our preference for Eq. (1a) (incipient motion of clasts) rather than Eq. (1b) (channel-forming floods).

4.1.2   Protrusion and hiding effects and consequences for the selection of ϕ values

Larger bed surface grains, as is the case for most of the imbricated clasts, may exert lower mobility thresholds because of a greater protrusion and a smaller intergranular friction angle, as noted by Buffington and Montgomery (1997) in their review. This has been explored through experiments and field-based investigations (e.g., Buffington et al., 1992; Johnston et al., 1998). These studies resulted in the notion that the entrainment of the largest clasts (e.g., the D_{84}) requires lower flow strengths than the shift in median-sized sediment particles. Accordingly, while ϕ values might be as high as 0.1 upon the displacement of the D_{50} (Buffington et al., 1992), conditions for the incipient dislocation of large clasts could be significantly different. In particular, for clasts that are up to five times larger than the D_{50} (which corresponds to the ratio between the D_{84} and the D_{50} of the Swiss data, Table 1), Buffington et al. (1992) and also Johnston et al. (1998) predicted ϕ values that might be as low as 0.03 or even less. Similar ϕ values, for instance, have indeed been applied for mountain streams where the supply of sediment from the lateral hillslopes has been large (Van den Berg and Schlunegger, 2012). This has been considered to result in a poor sorting and a low packing of the material and thus in low thresholds particularly for the incipient motion of large clast (Lenzi et al., 2006; Van den Berg and Schlunegger, 2012). Our calculations predict that an upper flow regime will not establish at these conditions (ϕ value of 0.03).

However, we consider it unlikely that the formation of most of the imbrication, as we encountered in the analyzed Alpine streams and in the stratigraphic record, was associated with thresholds as low as those proposed by e.g., Lenzi et al. (2006) and Van den Berg and Schlunegger (2012). We base our inference on the observation that the large clasts are generally well sorted and densely packed, both on subaerial (during low-water stages) and subaquatic bars. This results in a high interlocking degree within the bars we have encountered in the field. In addition, field inspections showed that the base of most of the large clasts, particularly those in subaquatic bars, are embedded and thus buried in finer-grained material, and only very few clasts are lying isolated and flat on their a–b planes. This implies that the fine-grained material has to be removed before these clasts can be entrained. In this case, hiding effects associated with ϕ values > 0.5 would possibly be appropriate for the prediction of material entrainment (Buffington and Montgomery, 1997). Accordingly, a dislocation of the large clasts and thus a rearrangement of the sedimentary fabric most likely requires high-discharge events with large flow strengths, because large thresholds have to be exceeded. We thus propose that a ϕ value of ca. 0.05, which is commonly used for the entrainment of the D_{50} (Paola and Mohring, 1996), is also adequate for predicting the hydrological conditions in Alpine streams at the onset of grain motion. We do acknowledge, however, that this hypothesis warrants a test with quantitative data, which is currently not available. Please note that the low Froude numbers and thus the low ϕ values of 0.3 inferred for the Thur and the Birse streams might be underestimates, because photos taken during high-stage flows display clear evidence for multiple hydraulic jumps over meter-long reaches in these streams (Spreafico et al., 2001, p. 71 and p. 77).

4.1.3 Variations in channel gradient at the bar and reach scales

Figure 3 shows that the results largely hinge on the values of ϕ and S. We applied Eq. (3) while inferring a steady uniform flow and a bed slope, which is constant over a distance of 500 m. We did not consider any smaller-scale slope variations associated with alternations of bars, riffles and pools as we lack the required quantitative information. Our simplification results in an energy slope, which is neither equal to the water surface slope nor to the bed slope. Such inequalities increase substantially when unsteady non-uniform supercritical flows and transitions are considered (e.g., Fig. 1a). This is not fully described by Eqs. (3) and (4) and thus introduces a bias. Similar variations in bar morphologies are not depicted in experiments either (e.g., Buffington et al., 1992; Powell et al., 2016), which could partially explain the low ϕ values that result from these studies. We justify our simplification because we are mainly interested in exploring whether supercritical flows are likely to occur for particular ϕ and channel gradient values.

4.2 Relationships between channel gradient, bed roughness and flow regime

We have found an expression where the Froude number F, and thus the change from the lower to the upper flow regime, depends on the channel gradient S and the bed roughness D_{84}/d (Eq. 7). This relationship also predicts that the controls of both parameters on the Froude number are to some extent independent from each other. Under these considerations, the similar patterns on Fig. 3 are unexpected. However, we note that we computed both relationships for the case of the incipient motion of the D_{84}. This threshold is explicitly considered by Eq. (2), which we used as basis to derive an expression where the Froude number F depends on the channel gradient or the bed roughness only. Therefore, it is not surprising that the dependency of F on gradient and bed roughness follows the same trends. In addition, Blissenbach (1952), Paola and Mohring (1996) and also Church (2006) showed that channel gradient, water depth and grain size are closely related during the entrainment of sediment particles. In particular, channels with coarser-grained gravel bars tend to be steeper and shallower than those where the bed material is finer grained (Church, 2006). In the same sense, bed roughness tends to be larger in steeper streams than in flatter channels (Whipple, 2004). We use the causal relationships between these variables to explain the similarities in Fig. 3a and b.

The tendency towards lower Froude numbers for a channel gradient $>1°$ ($\phi > 0.05$) and a bed roughness > 0.3 ($\phi > 0.05$) is somewhat unexpected. We explain these trends through the nonlinear relationships between slope, water depth, the energy loss within the roughness layer, and the velocity at the flow's surface.

4.3 The formation of imbrication in experiments

Interpretations of the possible linkages between hydrological conditions upon material transport and the formation of imbrication are hampered because experiments have not been designed to explicitly explore these relationships. In addition, as noted by Carling et al. (1992), natural systems differ from experiments because of the contrasts in scales. Nevertheless, many experiments have reproduced clast imbrication in subcritical flumes (Carling et al., 1992) or even in stationary flows (Aberle and Nikora, 2006). For instance, imbrication was reproduced at low Froude numbers between ca. 0.55 and 0.9 (Powell et al., 2016; Bertin and Friedrich, 2018), or at least during some non-specified subcritical flow (Johansson, 1963). Note that we inferred the Froude numbers from the experimental setup of these authors. Also in experiments, material transport occurred at ϕ values as low as 0.03 (Powell et al., 2016), which is consistent with the low Froude numbers for some of the streams in Switzerland. Based on field observations, Sengupta (1966) reported examples where pebbles embedded in sand started to imbricate during lower

regime flows. In these examples, eddies developed at the up-stream end of pebbles, which then lead to the winnowing of the fine-grained sand at the upstream edge and the tilting of this particular clast. Additional sliding, pivoting and vibrating of these sediment particles then resulted in the final imbrication. If this process occurs multiple times and affects the sand–gravel interface at various sites, then an armored bed with imbricated clasts can establish without the necessity of supercritical flows, or changes in flow regimes, as experimental results have shown (Aberle and Nikora, 2006; Haynes and Pender, 2007). Such a fabric may even form in response to prolonged periods of sub-threshold flows, as summarized by Ockelford and Haynes (2013). Also through flume experiments in a 0.3 m wide, 4 m long, recirculating tilting channel flume, Brayshaw (1984) was able to reproduce cluster bedforms with imbricated clasts during subcritical flows (F numbers between 0.03 and 0.07). In addition to these complexities, Carling et al. (1992) showed that the shape of a clast has a strong control on the thresholds for incipient motion, the style of motion and the degree of imbrication.

However, inspections of photos illustrating the experimental setup reveal that the surface grains are either flat lying on finer-grained sediments before their entrainment (Fig. 3 in Powell et al., 2016), occur isolated on the ground (Fig. 2.1b in Carling et al., 1992), or have a low degree of interlocking (Fig. 3a in Lamb et al., 2017). Interestingly, the experiment by Buffington et al. (1992) followed a different strategy, where a natural bed surface of a stream was peeled off with epoxy. They subsequently used this peel in the laboratory to approximate a natural channel bed surface (see their Fig. 4), on top of which they randomly placed grains with a known size distribution. Buffington and co-authors then measured the friction angle of the overlying grains, based on which they calculated the critical boundary shear stress values ϕ. In all experiments, the surface morphology lacks topographic variations, which we found as reach-scale alternations of riffles, transverse bars and pools in the field. The low ϕ values of 0.03, which appears to be typical of bed surfaces in laboratory flumes (Ferguson, 2012), as summarized by Powell et al. (2016), could possibly be explained by these conditions. Furthermore, and probably more relevant, the experimental reaches are quite short in comparison to natural settings and range between 4.0 m (Brayshaw, 1984), 4.4 m (Powell et al., 2016), 15 m (e.g., Lamb et al., 2017) and 20 m (Aberle and Nikora, 2006). We acknowledge that in most experiments the variables have been normalized through a constant Reynolds or Froude number (Brayshaw, 1984). This normalization also includes the experimental D_{50} grain sizes, which are very similar to those of our streams (Litty and Schlunegger, 2017). Nevertheless, we find it really hard to upscale some of the experimental results to our natural cases where standing waves of 1 m, and even between 5 and 8 m lengths, may occur (our Figs. 1b, 5b, 6b, Supplement), which are not reproducible in experiments. In addition, Powell et al. (2016) observed that the water surface stayed relatively stable during

their experiments and that the flows were steady and uniform without hydraulic jumps. This contrasts to our natural cases where upper and lower flow regimes alternate over short distances even during low-stage flows. Finally, while winnowing of fine-grained material, tilting and imbrication of clasts and subsequent bed armoring might be valuable mechanisms during subcritical flows in experiments, we consider it unlikely that this can be directly translated to our field observations. We base our inference on two closely related arguments. First, our reported groups of imbricated clasts tend to be arranged as cluster bedforms (e.g., Figs. 6d, 7b), which rather form in response to selective deposition of large clasts (Brayshaw, 1984) than selective entrainment of fine-grained material (Fig. 6a). Second, observations (Berther, 2012) and calculations (Litty and Schlunegger, 2017) have shown that effective sediment transport in these streams is likely to occur on decadal timescales (and most likely much shorter; Van den Berg and Schlunegger, 2012), at least for subaquatic bars. Sediment transport is then likely to occur over a limited reach only. This means that a large fraction of the shifted material per flood has a local source situated in the same river some hundreds of meters farther upstream where bars are also well armored. This possibly calls for large thresholds for the removal of clasts. In addition, on subaerial bars, fine-grained material is deposited and not winnowed during waning stages of floods, as our observations have shown. Accordingly, while low ϕ values and thus a lower flow regime might be appropriate for predicting the entrainment of sediment particles in experiments, greater thresholds and thus larger ϕ values are likely to be appropriate for our natural examples for the reasons we have explained above.

4.4 Relationships between flow regime and clast imbrication in the field

Here, we provide evidence for linking clast imbrication with supercritical flows provided that gravels are well sorted and densely packed and form a clast-supported fabric. We sustain our inferences with (i) published examples from natural environments, (ii) our observations from Swiss streams and (iii) the results of our calculations.

For the North Saskatchewan River in Canada, Shaw and Kellerhals (1977) reported gravel mounds on a lateral gravel bar with a spacing between 2 and 3 meters and a relatively flat top. Shaw and Kellerhals considered these bedforms as antidunes, which might have formed in the upper flow regime. In the same sense, transverse ribs were considered as evidence for the deposition either under upper flow regime conditions or in response to upstream-migrating hydraulic jumps (e.g., Koster, 1978; Rust and Gostin, 1981). These features have been described from modern streams as a series of narrow, current-normally orientated accumulations of large clasts. Koster (1978) additionally reported that transverse ribs are associated with clast imbrication (Fig. 2 in Koster, 1978). Alexander and Fielding (1997) found modern

gravel antidunes with well-developed clast imbrication in the Burdekin River, Australia. Finally, Taki and Parker (2005) reported cyclic steps of channel floor bedforms with wavelengths 100–500 times larger than the flow thickness. These bedforms most likely represent chute-and-pool configurations (Taki and Parker, 2005), which could have formed in response to alternations of upper and lower flow regime conditions, as outlined by Grant (1997). In such a situation, the upstream flow on the stoss side of the bedform experiences a reduction of the flow velocity, with the effect that the flow may shift to subcritical conditions. This would be associated with a hydraulic jump and a flow velocity reduction and thus with a drop of shear stresses (Fig. 1a), which could result in the deposition of clasts. In such a scenario, the site of sediment accumulation most likely migrates upstream (Fig. 8).

Our inspections of modern gravel bars and stratigraphic records (Fig. 4) reveal the occurrence of imbrication where channel slopes are steeper than 0.4°–0.5° , and where the values of bed roughness exceed ca. 0.06. The results of our generic calculations (Fig. 3) reveal that flows might become supercritical under these conditions, provided ϕ is greater than ca. 0.05 (Fig. 3). This is supported by observations form the Waldemme and Reuss rivers (slope > 0.5°) during high- and low-stage flows (Figs. 5b and 6b) that provide evidence for standing waves and thus supercritical flows (supplement). Contrariwise, the reach of the Emme river is flatter (slope < 0.4°), imbrication is largely absent and flows are generally subcritical (Sprefacio et al., 2001, p. 53). We thus propose that a channel gradient of ca. 0.5° is critical for both the formation of clast imbrication and possibly also for the establishment of supercritical flows. Based on these relationships, we suggest that the generation of imbrication occurs at upper flow regime conditions.

The proposed threshold slope is consistent with the results of previous work, where upper flow regime bedforms such as transverse ribs have been described for the Peyto outwash (slope ca. 1.09°), the Spring Creek (same slope; McDonald and Banerjee, 1971) and the North Saskatchewan River (slope 0.52°; Department of Mines and Technology Surveys, 1957). This is also in agreement with observations (Mueller et al., 2005) and the results of theoretical work calibrated with data (Lamb et al., 2008). In particular, Mueller et al. (2005) suggested that a ϕ value of ca. 0.03 is suitable for slopes < 0.35°, while $\phi > 0.1$ might be more appropriate for the mobilization of coarse-grained material in channels steeper than 1.1°. This might be an overestimate of the ϕ dependency of the slope (Lamb et al., 2008), but it does show that ϕ values larger than 0.04 and 0.05 might be appropriate where channels are steep (see also Ferguson, 2012). Finally, Simons and Richardson (1960, p. 45) noted that flows rarely exceed unity Froude numbers over an extended period of time in a stream with erodible banks. We thus use the conclusion of these authors to explain the limited spatial extent of imbricated clasts in modern streams and stratigraphic records.
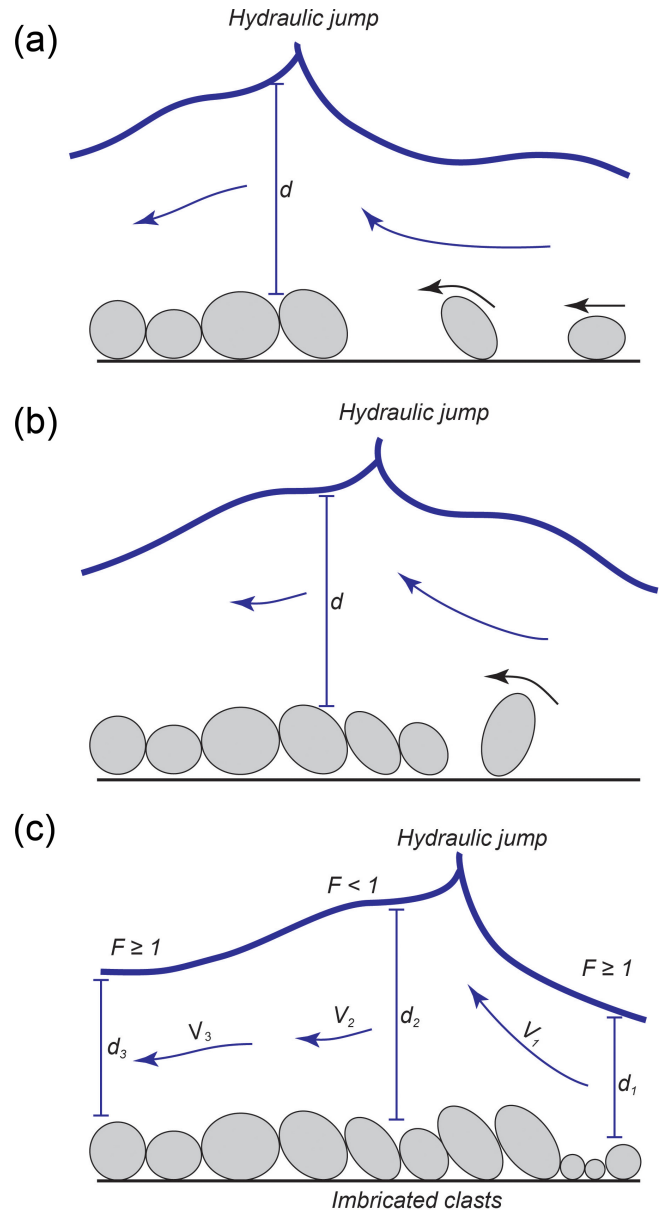

Figure 8. Conceptual sketch illustrating the formation of an ensemble of imbricated clasts as time proceeds (**a** through **c**). According to this model, the site of sediment accumulation will migrate upstream. F is the Froude number; v is the flow velocity; d is the water depth.

5   Summary and conclusions

We started with the hypothesis that the transport and deposition of coarse-grained particles, and particularly the formation of an imbricated fabric, may be related to changes in flow regimes. We then calculated the Froude number F at conditions of incipient motion of coarse-grained bedload for various bed roughness and stream gradient values, and we compared the results with data from modern streams and stratigraphic records. The results suggest that imbrication is

likely to provide evidence for supercritical conditions particularly where channels are steeper than $\sim 0.5°$ and where ϕ values are greater than ca. 0.05. We do acknowledge that our field-based inferences are associated with large uncertainties regarding channel gradients and grain size (Litty and Schlunegger, 2017) and that they lack a quantitative measure of the spatial distribution of clast imbrication (Bertin and Friedrich, 2018). In the same sense, our hydrologic calculations are based on the simplest published relationships between water flow and sediment transport. Greater complexities about material transport (Engelund and Hansen, 1967) have not been considered. This includes, for instance, large supply rates of sediment (Van den Berg and Schlunegger, 2012; Bekaddour et al., 2013); changes in bed morphology; spatial variations in turbulences; the shape and the sorting of grains; the 3-D arrangement of clasts (Lamb et al., 2008; Hodge et al., 2009); and complex hydrological conditions including upper-stage plain beds, hydraulic drops and standing waves (Johansson, 1963). In addition, the occurrence or absence of imbrication also depends on the shape of the involved clasts (Carling et al., 1992), where a relatively large c axis tends to form a steeper imbrication compared to a short c axis. In addition, experiments showed that spheres and rods have a higher mobility than blades and discs (Hattingh and Illenberger, 1995). Unfortunately, we lack the quantitative dataset to properly address these points. We also acknowledge that imbrication is formed in experiments under subcritical flows with low ϕ values (Brayshaw, 1984; Carling et al., 1992; Powell et al., 2016; Lamb et al., 2017). However, as already noted above, we find it quite hard to upscale the experimental results (< 20 m) to the reach scale of our observations where standing waves with wavelengths as long as 8 m have been observed (Fig. 6b, Supplement).

Despite our simplifications, we find evidence for proposing that the formation of imbrication likely occurs at supercritical conditions provided that (i) channels are steeper than ca. $0.5° \pm 0.1°$; and (ii) large clasts are tightly packed, closely arranged as cluster bedforms and partly embedded in finer-grained sediment. Mobilization and rearrangement of these structures require greater thresholds (Brayshaw, 1985), which might be large enough (ϕ values possibly > 0.05) to allow supercritical conditions to occur. These findings might be useful for the quantification of hydrological conditions recorded in the stratigraphic record such as conglomerates. As a further implication, the occurrence of imbrication in geological archives may be used to infer a minimum paleotopographic slope of $0.5° \pm 0.1°$ at the time the sediments were deposited. Such a constraint might be beneficial for paleogeographic reconstructions and for the subsidence analysis of sedimentary basins (e.g., Schlunegger et al., 1997). Finally, for modern streams, the presence of imbrication on gravel bars might be more conclusive for inferring an upper flow regime upon material transport than other bedforms such as transverse ribs or antidunes (Koster, 1978; Rust and

Gostin, 1981), mainly because clast imbrication has a better preservation potential and is easier to recognize in the field.

The Supplement related to this article is available online at https://doi.org/10.5194/esurf-6-743-2018-supplement.

Author contributions. FS designed the study and carried out the calculations, PG and FS collected the data, FS wrote the text with contributions by PG, and both authors contributed to the analyses and discussion of the results.

References

Aberle, J. and Nikora, V., Statistical properties of armored gravel bed surfaces, Water Resour. Res., 42, W11414, https://doi.org/10.1029/2005WR004674, 2006.

Allen, P. A., Earth Surface Processes, John Wiley and Sons, Oxford, 416 pp., 1997.

Alexander, J. and Fielding, C.: Gravel antidunes in the tropical Burdekin River, Queensland, Australia, Sedimentology, 44, 327–337, 1997.

Alexander, J., Bridge, J. S., Cheel, R. J., and Leclair, S. F.: Bedforms and associated sedimentary structures formed under supercritical water flows over aggrading sand beds, Sedimentology, 48, 133–152, 2001.

Andrews, E. D.: Bed-material entrainment and hydraulic geometry of gravel-bed rivers in Colorado, GSA Bull., 95, 371–378, 1984.

Bekaddour, T., Schlunegger, F., Attal, M., and Norton, P. K.: Lateral sediment sources and knickzones as controls on spatio-temporal variations of sediment transport in an Alpine river, Sedimentology, 60, 342–357, 2013.

Berther, R.: Geomorphometrische Untersuchungen entlang der Entle, Ms. Thesis, Univ. Bern, Bern, Switzerland, 94 pp., 2012.

Bertin, S. and Friedrich, H.: Effect of surface texture and structure on the development of stable fluvial armors, Geomorphology, 306, 64–79, 2018.

Blissenbach, L.: Relation of surface angle distribution to particle size distribution on alluvial fans, J. Sediment. Petrol., 22, 25–28, 1952.

Bray, D. I. and Church, M.: Armored versus paved gravel beds. J. Hydraul. Div., 106, 1937–1940, 1980.

Brayshaw, A. C.: Characteristics and origin of cluster bedforms in coarse-grained alluvial channels, in: Sedimentology of Gravels and Conglomerates, edited by: Koster, E. H., and Steel, R. J., Mem. Can. Soc. Petrol. Geol., 10, 77–85, 1984.

Brayshaw, A. C.: Bed microtopography and entrainment thresholds in gravel-bed rivers, GSA Bull., 96, 218–223, 1985.

Buffington, J., Dietrich, W. E., and Kirchner, J. W.: Friction angle measurements on a naturally formed gravel streambed: Implications for critical boundary shear stress, Water Resour. Res., 28, 411–425, 1992.

Buffington, J. M. and Montgomery, D. R.: A systematic analysis of eight decades of incipient motion studies, with special reference to gravel-bedded rivers, Water Resour. Res., 33, 1993–2029, 1997.

Carling, P. A.: Armored versus paved gravel beds – discussion, J. Hydraul. Div., 107, 1117–1118, 1981.

Carling, P. A., Kelsey, A., and Glaister, M. S.: Effect of bed roughness, particle shape and orientation on initial motion criteria, in: Dynamics of gravel-bed rivers, edited by: Billi, P., Hey, R. D., Throne, C. R., and Tacconi, P., 23–39, John Wiley and Sons, Ltd., Chichester, 1992.

Church, M.: Palaeohydrological reconstructions from a Holocene valley fill, Fluvial sedimentology, edited by: Miall, A. D., Mem. Can. Soc. Petrol. Geol., 5, 743–772, 1978.

Church, M.: Bed material transport and the morphology of alluvial river channels, Ann. Rev. Earth Planet. Sci., 34, 325–354, 2006.

D'Arcy, M., Roda-Boluda, D. C., and Whittaker, A. C.: Glacial-interglacial climate changes recorded by debris flow fan deposits, Owens Valley, California, Quat. Sci. Rev., 169, 288–311, 2017.

Department of Mines and Technology Surveys, Atlas of Canada, Geogr. Branch, Ottawa, 1957.

Duller, R. A., Whittaker, A. C., Swinehart, J. B., Armitage, J. J., Sinclair, H. D., Bair, A., and Allen, P. A., Abrupt landscape change post-6Ma on the central Great Plains, USA, Geology, 40, 871–874, 2012.

Egiazaroff, I. V.: Calculation of nonuniform sediment concentrations, J. Hydraul. Eng., 91, 225–247, 1965.

Engesser, B. and Kälin, D.: *Eomys helveticus* n. sp. and *Eomys schluneggeri* n. sp., two new small eomyids of the Chattian (MP 25/MP 26) subalpine Lower Freshwater Molasse of Switzerland, Fossil Imprint, 73, 213–224, 2017.

Engelund, F. and Hansen, E.: A monograph on sediment transport in alluvial streams, Teknisk Forlag, Copenhagen, 62 pp., 1967.

Ferguson, R.: Flow resistance equations for gravel- and boulder- bed streams. Water Resour. Res., 43, W05427, https://doi.org/10.1029/2006WR005422, 2007.

Ferguson, R.: River channel slope, flow resistance, and gravel entrainment thresholds, Water Resour. Res., 48, W05517, https://doi.org/10.1029/2011WR010850, 2012.

Garefalakis, P. and Schlunegger, F.: Link between concentrations of sediment flux and deep crustal processes beneath the European Alps, Sci. Rep., 8, 183, https://doi.org/10.1038/s41598-017-17182-8, 2018.

Grant, G. E., Swanson, F. J., and Wolman, M. G.: Pattern and origin of stepped-bed morphology in high gradient streams, western Cascades, Oregon, GSA Bull., 102, 340–352, 1990.

Grant, G. E.: Critical flow constrains flow hydraulics in mobile-bed streams: A new hypothesis, Water Resour. Res, 33, 349–358, 1997.

Hattingh, J. and Illenberger, W. K.: Shape sorting of flood-transported synthetic clasts in a gravel bed river, Sed. Geol., 96, 181–190, 1995.

Haynes, H. and Pender, G.: Stress history effects on graded bed stability, J. Hydraul. Eng., 33, 343–349, 2007.

Hey, R. D. and Thorne, C. R.: Stable channels with mobile gravel beds, J. Hydrol. Eng., 112, 671–689, 1986.

Hodge, R., Brasington, J., and Richards, K.: In situ characterization of grain-scale fluvial morphology using Terrestrial Laser Scanning, Earth Surf. Process. Landf., 34, 954–968, 2009.

Howard, A. D., in: Thresholds in Geomorphology, edited by: Coates, D. R. and Vitek, J. D., Allen and Unwin, Boston, MA, 227–258, 1980.

Jarrett, R. D.: Hydraulics of high-gradient streams, J. Hydr. Eng., 110, 1519–1939, 1984.

Johansson, C. E.: Orientation of pebbles in running water: a laboratory study, Geogr. Ann., 45, 85–112, 1963.

Johnston, C. E., Andrews, E. D., and Pitlick, J.: In situ determination of particle friction angles of fluvial gravels, Water Resour. Res., 34, 2017–2030, 1998.

Kempf, O., Matter, A., Burbank, D. W., and Mange, M.: Depositional and structural evolution of a foreland basin margin in a magnetostratigraphic framework; the eastern Swiss Molasse Basin, Int. J. Earth Sci., 88, 253–275, 1999.

Kirchner, J. W., Dietrich, W. E., Iseya, F., and Ikeda, H.: The variability of critical shear stress, friction angle, and grain protrusion in water-worked sediments, Sedimentology, 37, 647–672, 1990.

Koster, E. H.: Transverse ribs: their characteristics, origin and paleohydrauic significance, in: Fluvial sedimentology, edited by: Miall, A. D., Mem. Can. Soc. Petrol. Geol., 5, 161–186, 1978.

Krogstad, P. A. and Antonia, R. A.: Surface roughness effects in turbulent boundary layers, Exp. Fluids, 27, 450–460, 1999.

Lamb, M. P., Dietrich, W. E., and Venditti, J. G.: Is the critical Shields stress for incipient sediment motion dependent on channel bed slope?, J. Geophys. Res., 113, F02008, https://doi.org/10.1029/2007JF000831, 2008.

Lamb, M. P., Brun, F., and Fuller, B. M.: Hydrodynamics of steep streams with planar coarse-grained beds: Turbulence, flow resistance, and implications for sediment transport, Water Resour. Res., 53, 2240–2263, 2017.

Lenzi, M. A., Mao, I., and Comiti, F.: When does bedload transport begin in steep boulder-bed streams?, Hydrol. Proc., 20, 3517–3533, 2006.

Litty, C. and Schlunegger, F.: Controls on pebbles' size and shapes in streams of the Swiss Alps, J. Geol., 123, 405–427, 2017.

Matter, A.: Sedimentologische Untersuchungen im östlichen Napfgebiet (Entlebuch – Tal der Grossen Fontanne, Kt. Luzern), Eclogae Geol. Helv., 57, 315–428, 1964.

McDonald, B. C. and Banerjee, I.: Sediments and bedforms on a braided outwash plain, Can. J. Earth Sci., 8, 1282–1301, 1971.

Meyer-Peter, E. and Müller, R.: Formulas for bedload transport, Proceedings of the 2nd meeting of the Int. Assoc. Hydraul. Struct. Res., Stockholm, Sweden, Appendix 2, 39–64, 1948.

Miall, A. D.: Fluvial sedimentology: An historical overview, in: Fluvial sedimentology, edited by: Miall, A. D., Mem. Can. Soc. Petrol. Geol., 5, 1–48, 1978.

Middleton, L. T. and Trujillo, A. P.: Sedimentology and depositional setting of the upper Proterozoic Scanlan Conglomerate, central Arizone, in: Sedimentology of gravels and conglomerates, edited by: Koster, E. H. and Steel, R. J., Mem. Can. Soc. Petrol. Geol., 10, 189–202, 1984.

Mueller, E. R., Pitlick, J., and Nelson, J. M.: Variation in the reference Shields stress for bed load transport in gravel-bed streams and rivers, Water Resour. Res., 41, W04006, https://doi.org/10.1029/2004WR003692, 2005.

Ockelford, A.-M. and Haynes, H.: The impact of stress history on bed structure, Earth Surf. Process. Landf., 38, 717–727, 2013.

Papaevangelou, G., Evangelides, C., and Tsimopoulos, C.: A new explicit relation for friction coefficient f in the Darcy-Weisbach equation, Proc. 10th Conf. Prot. Restor. Env., PRE10, Aristotle University of Thessaloniki, Greece, 6–9 July, 2010.

Paola, C. and Mohring, D.: Palaeohydraulics revisted: palaeoslope estimation in coarse-grained braided rivers. Basin Res., 8, 243–254, 1996.

Paola, C., Heller, P. L., and Angevine, C.: The large-scale dynamics of grain-size variation in alluvial basins, 1: Theory, Basin Res., 4, 73–90, 1992.

Parker, G.: Self-formed straight rivers with equilibrium banks and mobile bed. Part 2. The gravel river, J. Fluid Mech., 89, 127–146, 1978.

Parker, G., Klingeman, P. C., and McLean, D. G.: Bedload and size distribution in paved gravel-bed streams, J. Hydraul. Div. Am. Sco. Civ. Eng., 108, 544–571, 1982.

Pettijohn, F. J.: Sedimentary rocks, Harper and Brothers, New York, 718 pp., 1957.

Pfeiffer, A. M., Finnegan, N. J., and Willenbring, J. K.: Sediment supply controls equilibrium channel geometry in gravel rivers, P. Natl. Acad. Sci. USA, 114, 3346–3351, 2017.

Philips, C. B. and Jerolmack, D. J.: Self-organization of river channels as a critical filter on climate signals, Science, 352, 649–697, 2016.

Potsma, G. and Roep, T., Resedimented conglomerates in the bottomsets of Gilbert-type gravel deltas, J. Sed. Petrol., 55, 874–885, 1985.

Powell, M. D., Ockleford, A., Rice, S. P., Hillier, J. K., Nguyen, T., Reid, I., Tate, N. J., and Ackerley, D.: Structural properties of mobile armors formed at different flow strengths in gravel-bed rivers. J. Gephys. Res. – Earth Surface; 121, 1494–1515, 2016.

Rust, B. R., Depositional models for braided alluvium, in: Fluvial sedimentology, edited by: Miall, A. D., Mem. Can. Soc. Petrol. Geol., 5, 221–245, 1978.

Rust, B. R.: Proximal braidplain deposits in the Middle Devonian Malbaie Formaiton of eastern Gaspé, Quebec, Canada, Sedimentology, 31, 675–695, 1984.

Rust, B. R. and Gostin, V. A.: Fossil transverse ribs in Holocene alluvial fan deposits, Depot Creek, South Australia, J. Sediment. Petrol., 51, 441–444, 1981.

Schlunegger, F. and Castelltort, S.: Immediate and delayed signal of slab breakoff in Oligo/Micoene Molasse deposits from the European Alps, Sci. Rep. 6, 31010, https://doi.org/10.1038/srep31010, 2016.

Schlunegger, F. and Norton, K. P.: Climate vs. tectonics: the competing roles of Late Oligocene warming and Alpine orogenesis in constructing alluvial megafan sequences in the North Alpine foreland basin, Basin Res., 27, 230–245, 2015.

Schlunegger, F., Burbank, D. W., Matter, A., Engesser, B., and Mödden, C.: Magnetostratigraphic calibration of the Oligocene to Middle Miocene (30–15 Ma) mammal bizones and depositional sequences of the central Swiss Molasse basin, Eclogae geol. Helv., 89, 753–788, 1996.

Schlunegger, F., Jordan, T. E., and Klaper, E. M.: Controls of erosional denudation in the orogeny on foreland basin evolution: The Oligocene central Swiss Molasse Basin as an example, Tectonics, 16, 823–840, 1997.

Schlunegger, F., Norton, K. P., Delunel, R., Ehlers, T. A., and Madella, A.: Late Miocene increase in precipitation in the Western Cordillera of the Andes between 18-19° latitudes inferred from shifts in sedimentation patterns, Earth Planet. Sci. Lett., 462, 157–168, 2017.

Sengupta, S.: Studies on orientation and imbrication of pebbles with respect to cross-stratification, J. Sed. Petrol., 36, 227–237, 1966.

Shaw, J. and Kellerhals, R.: Paleohydraulic interpretation of antidune bedforms with applications to antidunes in gravel, J. Sediment. Petrol., 47, 257–266, 1977.

Shields, A.: Andwendungen der Aehnlichkeitsmechanik und der Turbulenzforschung auf die Geschiebebewegung, Mitt. Preuss. Versuch. Wasserbau Schiffbau, 26 pp., Berlin, 1936.

Simons, E. V. and Richardson, E. V.: Discussion of resistance properties of sediment-laden streams, Am. Soc. Civil Eng. Trans., 125, 1170–1172, 1960.

Sinclair, H. D. and Jaffey, N.: Sedimentology of the Indus Group, Ladakh, northern India: implications for the timing of initiation of the paaeo-Indus River, J. Geol. Soc. London, 158, 151–162, 2001.

Slootman, A., Simpson, G., Castelltort, S., and De Boer, P. L.: Geological record of marine tsunami backwash: The role of the hydraulic jump, Depositional Record, 1–19, 2018.

Spicher, A.: Geologische Karte der Schweiz 1 : 500'000, Schweiz. Natf. Ges., 1980.

Spreafico, M., Hodel, H. P., and Kaspar, H.: Rauheiten in ausgesuchten schweizerischen Fliessgewässern, Berichte des BWG, Seri Wasser, 102 pp., Bern, 2001.

Stürm, B.: Die Rigischüttung. Sedimentpetrographie, Sedimentologie, Paläogeographie, Tektonik, PhD thesis, Univ. Zürich, Switzerland, 98 pp., 1973.

Taki, K. and Parker, G.: Transportational cyclic steps cre- ated by flow over an erodible bed. Part 1. Experiments, J. Hydrol. Res., 43, 488–501, 2005.

Todd, S. P.: Process deduction from fluvial sedimentary structures, in: Advances in fluvial dynamics and stratigraphy, edited by: Carling, P. A. and Dawson, M. R., John Wiley & Sons Ltd, 299–350, 1996.

Trieste, D. J.: Evaluation of supercritical/subcritical flows in high-gradient channel, J. Hydr. Eng., 118, 1107–1118, 1992.

Trieste, D. J.: Supercritical flows versus subcritical flows in natural channels, in: Hydraulic Engineering '94: Proceedings of the 1994 Conference of the Hydraulics Division, edited by: Cotroneo, G. V. and Rumer, R. R., Am. Soc. Civ. Eng., New York, 732–736, 1994.

Tucker, G. and Slingerland, R., Drainage basin responses to climate change, Water Resour. Res., 33, 2031–2047, 1997.

Van den Berg, F. and Schlunegger, F.: Alluvial cover dynamics in response to floods of various magnitudes: The effect of the release of glaciogenic material in a Swiss Alpine catchment, Geomorphology, 141, 121–133, 2012.

Whipple, K. X.: Bedrock rivers and the geomorphology of active orogens, Ann. Rev. Earth Planet. Sci., 32, 151–185, 2004.

Wiberg, P. L. and Smith, J. D.: Velocity distribution and bed roughness in high-gradient streams, Water Resour. Res., 27, 825–838, 1991.

Wickert, A. D. and Schildgen, T. F.: Long-Profile Evolution of Transport-Limited Gravel-Bed Rivers, Earth Surf. Dynam. Discuss., https://doi.org/10.5194/esurf-2018-39, in review, 2018.

Wong, M. and Parker, G.: Reanalysis and correction of bed-load relation of Meyer-Peter and Müller using their own database, J. Hydraul. Eng., 132, 1159–1168, 2006.

Yagishita, K.: Paleocurrent and fabric analyses of fluvial conglomerates of the Paeogene Noda Group, northeast Japan, Sed. Geol., 109, 53–71, 1997.